ELSEVIER

Biochimica et Biophysica Acta 1512 (2001) 53–63

BIOCHIMICA ET BIOPHYSICA ACTA
BBA

www.bba-direct.com

Lumen geometry of ion channels formed by *Vibrio cholerae* EL Tor cytolysin elucidated by nonelectrolyte exclusion

Liliya N. Yuldasheva [a], Petr G. Merzlyak [a], Alexander O. Zitzer [b], Cláudio G. Rodrigues [a], Sucharit Bhakdi [b], Oleg V. Krasilnikov [a,*]

[a] *Laboratory of Membrane Biophysics, Center of Biological Sciences, Department of Biophysics and Radiobiology, Federal University of Pernambuco, Av. Prof. Moraes Rego, S/N, Cidade Universitaria, 50670-901 Recife, PE, Brazil*
[b] *Institute of Medical Microbiology and Hygiene, Hochhaus am Augustusplatz, D-55101 Mainz, Germany*

Received 7 June 2000; received in revised form 15 February 2001; accepted 16 February 2001

Abstract

Vibrio cholerae EL Tor cytolysin, a water-soluble protein with a molecular mass of 63 kDa, forms small pores in target cell membranes. In this communication, planar lipid bilayers under voltage clamp conditions were used to investigate the geometric properties of the pores. It was established that all cytolysin channels were inserted into membranes with the same orientation. Sharp asymmetry in the I-V curve of fully open cytolysin channels persisting at high electrolyte concentrations indicated asymmetry in the geometry of the channel lumen. Using the nonelectrolyte exclusion method, evidence was obtained that the *cis* opening of the channel had a larger diameter ($\leq$1.9 nm) than the *trans* opening ($\leq$1.6 nm). The channel lumen appeared constricted, with a diameter of $\leq$1.2 nm. Cup-shaped lumen geometry was deduced for both channel openings, which appeared to be connected to each other via a central narrow part. The latter contributed significantly to the total electrical resistance and determined the discontinuous character of channel filling with nonelectrolytes. Comparisons of the properties of pores formed by cytolysins of two *V. cholerae* biotypes (EL Tor and non-O1) indicated that the two ion channels possessed a similar geometry.

Keywords: Cytolysin; Pore-forming toxin; Ion channel geometry; Nonelectrolyte exclusion technique; *Vibrio cholerae*

1. Introduction

Cytolysins produced by some *Vibrio cholerae* EL Tor strains and by most non-O1 strains are possible virulence factors [1,2]. These toxins are encoded by the hlyA gene [3–5], an 82 kDa protein which is then processed to an approx. 63 kDa mature cytolysin. The resulting N-terminal amino acid of the mature cytolysin depends on the protease that hydrolyzed the precursor [6]. The pathogenetic relevance of EL Tor cytolysin is not entirely clear; however, non-O1 *V. cholerae* strains that do not produce cholera toxin still cause illness [7–10] and a *V. cholerae* mutant lacking the cytolysin exhibited a 100-fold increase in LD_{50} (sucking mouse model) [11]. Thus the enteropathogenic action of those *V. cholerae* strains seems to be correlated with cytolysin production. Moreover, non-O1 *V. cholerae* strains that produce an EL Tor-related cytolysin also cause extraintestinal infections, including cellulitis, meningitis, wound infections and bacteremias [12–17].

* Corresponding author. Fax: +55-81-3271-8560; E-mail: kras@npd.ufpe.br

0005-2736/01/$ – see front matter
PII: S0005-2736(01)00302-9

Our previous studies have examined the action of EL Tor (VCC1) and non-O1 (VCC2) cytolysins on erythrocytes and nucleated cells [18–21]. Pore formation was considered responsible for enterotoxic [22] and lethal properties [1] of the cytotoxins. The channel-forming activity of cytolysins isolated from these two biotypes has been demonstrated in planar lipid bilayers [18,19,23]. Based on bilayer experiments, oligomerization was concluded to be an essential step in pore formation and a homooligomeric structure was suggested for the pore formed by both toxins. Most recently, the pentameric structure of VCC1 channels was established by SDS-PAGE analysis [24].

The geometry of the water-filled nanometer-scale pore largely defines the conductance, permeability for small molecules and in some degree the ion selectivity [25]. The geometry of the cytolysin transmembrane channel remains largely unknown. The diameter of the larger opening of the VCC2 channel in planar lipid bilayers and in erythrocyte membranes was estimated to be 1.8–2.0 nm using the nonelectrolyte polymer exclusion technique and osmotic balance method [18]. For VCC1 channels, the effective channel diameter (approx. 1.4–2.0 nm) was deduced from the channel conductance [23]. Channel geometry is likely to be closely linked with functional channel features and, consequently, with biological effects of the toxin. To obtain such information for the VCC1 channel, we employed a variation of the polymer-exclusion approach [26], which yielded data in excellent agreement with crystallographic data for *Staphylococcus aureus* α-toxin channel [27]. By this method, the influence of asymmetrically applied nonelectrolytes on channel conductance is analyzed in terms of channel pore geometry. Using this method we provide evidence that *V. cholerae* EL Tor cytolysin channels have asymmetric lumen geometry with channel openings of different diameters and a constriction inside the lumen.

2. Materials and methods

2.1. Bacterial strain

V. cholerae 01 EL Tor (KM 169 type strain) was used for cytolysin purification. This strain was negative in tests for cholera toxin and heat-stable enterotoxin. Cytolysin was prepared as previously described [19].

2.2. Chemicals

Phosphatidylcholine (type V-E) and cholesterol were purchased from Sigma and used as received. Ethylene glycol and glycerol were from Merck. Experiments employed polyethylene glycol (PEG) with average molecular masses of (Da): 300, 400, 1000, 1450 (Sigma); 600 (Riedel de Hahn); and 2000 (Aldrich). Hydrodynamic radii of nonelectrolytes closely related with early published data [28,29] were taken from [30,31] and were the following: 0.26 ± 0.02 ethylene glycol, 0.31 ± 0.02 glycerol, 0.60 ± 0.04 nm PEG300, 0.70 ± 0.04 nm PEG400, 0.78 ± 0.04 nm PEG600, 0.94 ± 0.04 nm PEG1000, 1.05 ± 0.04 nm PEG1450, 1.22 ± 0.04 nm PEG2000. Other chemicals were analytical grade.

2.3. Methods

Planar lipid bilayer membranes were formed by the method of Montal [32]. Electrical characteristics of planar lipid bilayer membranes (PLM) were measured under voltage clamp conditions as described elsewhere [33]. The *trans* compartment of the experimental chamber was connected to the virtual ground, and voltage pulses were applied to the *cis* compartment of the chamber, where cytolysin was also added. Double-distilled water was used to prepare all buffer solutions. Unless stated otherwise, standard solution used in the bilayer experiments contained 0.15 M NaCl and 0.005 M HEPES at pH 6.5, adjusted with NaOH.

To record the I-V curve of single VCC1 channels, long-lasting voltage pulses (20–30 s duration) were applied. To record the instant I-V curve, the transmembrane potential was initially increased stepwise from zero to −110 mV and then gradually increased to 110 mV (during a voltage ramp with duration of 200–250 ms). Finally, the transmembrane potential was returned stepwise to zero mV.

Cation-anion selectivity of VCC1 channels was evaluated by measuring the zero current potential with different concentrations of KCl on the two sides of the PLMs. A 3-fold gradient (150/50 mM; *cis*/*trans*) was usually used.

Geometric features of the channel were determined as recently described [26], using 20% (w/v) solutions of nonelectrolytes. In this method, different small nonelectrolytes are placed in contact with one of the openings of the channel, while impermeant large nonelectrolytes are in contact with the other side of the channel. The method is based on changes in ion channel conductance induced by the addition of specific nonelectrolytes to the bathing solutions, which decrease the conductivity of the solutions. To keep the ion/water molar ratio constant, polymers were added to the standard solution to 20% (w/v) concentration. The conductivity of each solution was measured with an HI 9033 multi-range conductivity meter (HANNA Instruments) at 25°C. It should be stressed here that for a given nonelectrolyte concentration, bulk conductivities of solutions were the same for all nonelectrolytes used, the difference for nonelectrolytes of different masses being within 3%. Ion activities in 20% nonelectrolyte solutions were measured with selective electrodes and were found to have increased by a factor of approx. 1.3 for PEG solutions. Increased ion activity in the presence of PEG is well documented [30,31,34–36] and consists with the binding of two or three water molecules per PEG repeat unit [37–40]. The influence of ethylene glycol and glycerol on ion activity was almost negligible.

A simple approach to polymer partitioning into a channel pore consists of regarding random polymer coils as flexible spheres of corresponding average hydrodynamic radius. However, at least in experiments with the α-toxin channel [27], highly flexible PEG molecules (with Kuhn's length of about several angstroms only) phenomenologically behave as hard spheres. The reason for this PEG behavior is unknown. The qualitative picture of polymer partitioning into the channel pore is intuitively clear: water-soluble polymers whose characteristic sizes are much smaller than pore diameter partition into the pore easily, while large polymers are excluded from the pore because of entropic and steric reasons. A quantitative description is hampered by the fact that a number of factors governing polymer partitioning into ion channel pores are poorly understood. Thus, the scaling theory failed to rationalize the sharp dependence of the PEG partition coefficient for a channel on polymer molecular mass even in the case of symmetric equilibrium conditions [41]. The hard sphere approach (in its original form) is also not able to describe well the PEG partition [41]; however, it becomes able to do so assuming a reasonable repulsion force between polymers in the case of symmetric equilibrium conditions and low ionic strength [27]. The latter condition is very important. It prevents a significant interaction between a polymer and a channel wall [27], and for this reason was used by us throughout our study. The reason for the appearance of the repulsion force between polymers is still poorly understood.

Because several theoretical issues concerning polymer partitioning into a channel pore are still unresolved even in the case of symmetric equilibrium conditions, we employed here an empirical approach to analyze the partitioning at the asymmetrical conditions. We assumed that, if the nonelectrolyte hydrodynamic radius is smaller than any opening of the channel, the nonelectrolyte partitions freely, occupying (with a concentration equal to its bulk concentration) all space available before the constriction of a smaller radius. If the nonelectrolyte hydrodynamic radius is larger than the pore opening radius, it does not partition into the pore at all. Hence, if nonelectrolytes enter the channel lumen of a given channel, the conductance of that channel decreases. On the other hand, molecules that do not enter the lumen should not significantly alter single channel conductance [30,31,34–36,42].

Different nonelectrolytes are used as molecular probes. The chosen condition does not allow interaction of the nonelectrolyte with the channel lumen wall. Mean values of single channel conductances and solution conductivities are used to establish the filling (F) of the channel with a nonelectrolyte through one of its openings. The filling (with correction on access resistance) was calculated as described elsewhere [26]:

$$F = \left(\frac{Cg_o - g_i}{g_i}\right) \Big/ \left(\frac{\chi_o - \chi_i}{\chi_i}\right)$$

where g_o is the single channel conductance in the basic solution, in which the NaCl concentration was increased by a factor of 1.3; g_i is the single channel conductance in the presence of a solution containing 20% (w/v) of an nonelectrolyte with access to the channel interior on one side only (g_i^{cis} or

g_i^{trans}); χ_o is the conductivity of the nonelectrolyte-free space in a nonelectrolyte solution. It was assumed to be equal to χ for a standard solution in case of ethylene glycol or glycerol and was increased by a factor 1.3 in the presence of PEG in solution [30,31,33,35,36,41]; χ_i is the conductivity of the solution containing 20% (w/v) of a given polymer; C is a coefficient determined as follows:

$$C = \frac{g_o^{acc}}{g_o^{acc} - g_o} \times \left(1 - \frac{g_i}{g_i^{acc}}\right)$$

where g^{acc} is the conductance of access zones, which in accordance with Hall [43] is determined to be $g^{acc} = 4r\chi$, the subscripts 'o' and 'i' indicate values obtained in the absence and in the presence of a nonelectrolyte; r is the radius of the *cis* and the *trans* openings separately.

The dependence of F on the hydrodynamic radii of different nonelectrolyte molecules can be used to determine the diameter of the openings of an ion channel, the geometry of the channel lumen and a possible constriction in it. The methodology allows establishing the maximal size of both channel openings and constriction (if it exists) with ± 0.1 nm accuracy. Localization of a constriction can be determined with less precision. Relatively small concentrations of NaCl were used in the channel-sizing experiment. Under these conditions, non-specific hydrophobic interactions between nonelectrolytes and the channel wall (that can be clearly seen at high salt concentrations [27,41,42]) are minimal [27].

3. Results

In accord with published data [18,19,23], addition of VCC1 to voltage-clamped PLM led to stepwise increases in bilayer conductance (Fig. 1, inset A). Each step reflected the formation of a single anion-selective channel ($P_{Cl}/P_K \approx 3$). Usually current steps were quite uniform in size although channels with a conductance that was considerably less than the main value of the channel were occasionally observed. We excluded these low conductance events in our further analysis. The line (drawn by Microcal Origin, version 5.0 software) indicates the theoretical normal distribution of the main pool of channel

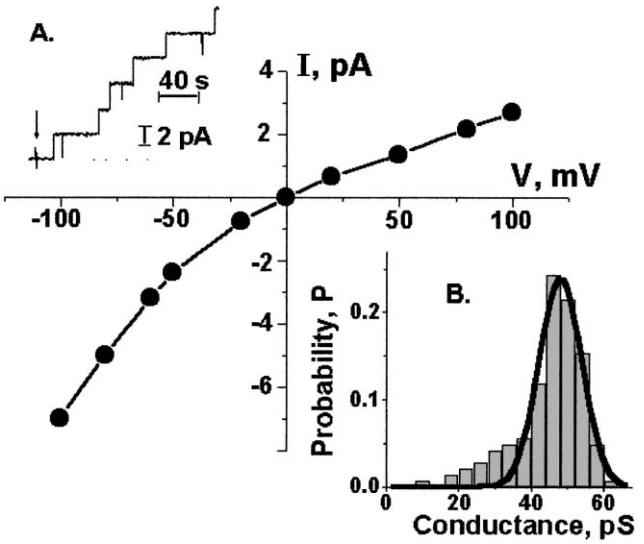

Fig. 1. The typical I-V curve of the single VCC1 channel in fully open state, a typical single-channel recording (inset A) and the histogram of single-channel conductance of VCC1 channels (inset B). Bilayer lipid membranes were formed from a phosphatidylcholine:cholesterol mixture 1:1 (by mass). Bathing solution contained 0.15 M NaCl, 0.005 M HEPES-NaOH buffer pH 6.5. VCC1 was always added to the *cis* compartment to a final concentration of approx. 0.4 μg/ml. The I-V curve of a single VCC1 channel like that shown in the current traces in inset A is represented. To build the I-V curve long-lasting voltage pulses (20–30 s duration) were applied. (Inset A) A typical single-channel recording of VCC1 channels. The bilayer was clamped at −50 mV. The dashed line indicates the zero current level, while the arrow indicates the addition of toxin. (Inset B) Histogram of the single-channel conductance of VCC1 channels. The probability, P, of observing conductance steps like those shown in the current traces in inset A is represented. Records were discarded if any of the open channels temporarily closed. The bilayer was clamped at −50 mV. More than 140 ion channels were registered (5–15 channels per membrane) under experimental conditions. Bin width was 4 pS. Line (drawn by Microcal Origin, version 5.0 software) indicates the theoretical normal distribution of the main pool of the channel events. All other conditions for the experiment are described in Section 2.

events (Fig. 1, inset B). The mean value of this distribution (peak) was taken as the single channel conductance for subsequent analysis. Under the chosen conditions, the mean single channel conductance was found to be 48.2 ± 5.9 pS. The apparently larger conductance found by Menzl et al. for VCC1 channels [23] may reflect the different pH and voltage used. pH is a significant factor for modifying all channel properties, particularly the shape of the I-V curve [18,44]. Of note, Menzl et al. used unbuffered salt

solutions [23]. The second, and perhaps main reason for the larger conductance in our study was the different value of voltage used. VCC1 channels [23], like VCC2 channels [18], exhibit sharp non-linearity and asymmetry of the I-V curve (Fig. 1). The shape of the I-V curve of the single VCC1 channel in the fully open state and that of the instant I-V curve of bilayers containing hundreds of channels were the same. Hence, the shape of the I-V curve reflected the intrinsic properties of the channel. The finding also indicated that all VCC1 channels are inserted in the same membrane orientation, and that individual VCC1 channels had identical asymmetry geometries and/or asymmetry charge distributions along their water lumen. Because I-V curve asymmetry could not be completely abolished by an increase in electrolyte concentration, the VCC1 channel could not be modeled as a simple cylinder. Rather, there evidently was some sort of structural heterogeneity inside the lumen of the channels. To examine this, the nonelectrolyte exclusion technique was employed.

To determine the size of each opening of the VCC1 channel and to obtain additional information about the geometry of the channel lumen, we measured channel conductances using specific nonelectrolytes in contact with either the *cis* or the *trans* channel openings. g^{cis} was almost always found to be larger than g^{trans}, which underscored a physical asymmetry in channel structure.

Starting with the smallest nonelectrolyte, increasing the hydrodynamic radius of a nonelectrolyte led to a progressive increase in g^{cis} as well as g^{trans}. The minimal size of the nonelectrolyte at which the maximal values g^{cis} and g^{trans} were reached corresponded to PEG600 and PEG1000 for *trans*- and *cis*-filling experiments, respectively. This result suggested that the two openings of the VCC1 channel were of different size.

To obtain a precise measurement of the radii of both channel openings and to acquire additional information on channel lumen geometry, it was necessary to analyze the dependence of channel filling on the nonelectrolyte hydrodynamic radius. As expected, F was dependent on the hydrodynamic radius of nonelectrolyte molecules (Fig. 2). In both cases, the maximal values of F (F_{max}) observed in the presence of the smallest nonelectrolyte (such as ethylene glycol and glycerol), were close to 0.9, indicating that

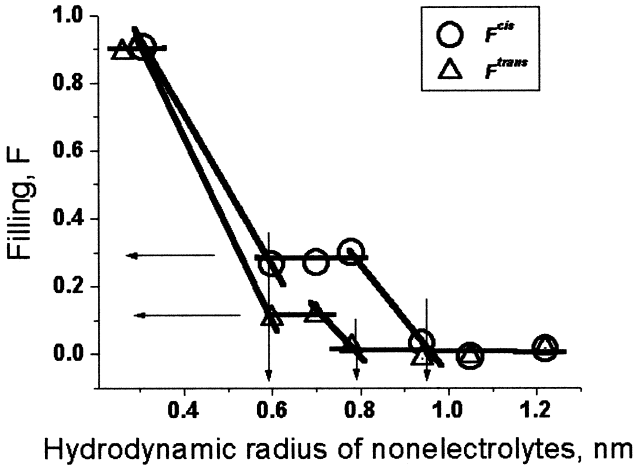

Fig. 2. The dependence of F^{cis} (○) and F^{trans} (△) on the hydrodynamic radii of nonelectrolytes. For *cis*-filling experiments, nonelectrolytes (20% w/v) were added at the *cis* opening of the channel, while impermeant nonelectrolyte (PEG2000, 20% w/v) was added to the *trans* side. For *trans*-filling experiments, nonelectrolytes (20% w/v) were added to the *trans* opening of the channel, while impermeant nonelectrolyte (PEG2000, 20% w/v) was added to the *cis* side. In both cases impermeant nonelectrolyte (PEG2000, 20% w/v) was used to decrease the osmotic pressure gradient across bilayers and, consequently, the directional water flux through VCC1 channels that can interfere with nonelectrolyte partitioning. More than 120 ion channels were registered (5–15 channels per membrane) under each experimental condition. These two maneuvers gave us two groups of cumulative histograms, which were analyzed in the same way as the control one (see Fig. 1). Mean values of VCC1 channel conductance in the presence of nonelectrolytes on the *cis* (g^{cis}) or *trans* (g^{trans}) side of the membrane were used to calculate F^{cis} and F^{trans} as described in Section 2. The error bars are equal or smaller than the symbols used. Vertical arrows indicate the radii values at critical points of the VCC1 channel. Division of F^{cis} and F^{trans} dependences into segments was made 'by eye'. The lowest horizontal segment was then fitted by first-order regression. Other segments were fitted by zero-order regressions. Horizontal arrows indicate filling values for the *cis* (≈ 0.3) and the *trans* (≈ 0.1) vestibules of the VCC1 channel, which ratios to the maximal observed filling (0.9) give apparent electrical distances from the openings to the constriction (for details see text). All other experimental conditions are as described in the legend to Fig. 1 and in Section 2.

the channels were readily permeated by these nonelectrolytes.

When a small nonelectrolyte (with a hydrodynamic radius considerably smaller than the radius of the pore) is applied to just one side of a cylindrical pore that is devoid of any constriction, it will be linearly diluted between both sides and its average concentration in the pore should be half of that in

the bulk, so that F_{max} would give 0.5. The larger experimentally obtained value of F (approx. 0.9) indicated that in both cases the apparent average concentration of these small nonelectrolytes in the pore was actually considerably larger than half and close to that in the bulk. At least two reasons could have been responsible for this: (1) interaction between nonelectrolyte and the channel lumen, or (2) divergence in the geometry of the VCC1 channel lumen from that of a cylinder [26,27,41,42]. Interaction between the nonelectrolyte and the channel wall could be excluded here because when nonelectrolytes were added simultaneously at both sides, we did not observe an F value above 1.0, as predictable for such an interaction [26,27]. Hence, we interpreted the finding to also indicate an essentially non-cylindrical geometry of the VCC1 channel lumen.

The above data would thus be consistent with the presence of an extensive constriction within the VCC1 channel, which would make a pivotal contribution to the channel conductance. In that confined space, nonelectrolyte diffusion can be limited [36] and the effective concentration of the smallest nonelectrolyte into the channel lumen will be close to that in the nonelectrolyte-containing bulk solution applied to just one side.

When nonelectrolytes with larger hydrodynamic radii were used, we observed different values for F^{cis} and F^{trans} experiments. This indicated asymmetry in VCC1 channel geometry. In both cases (in the *trans*- as well as in the *cis*-filling experiments), polymer partitioning showed biphasic behavior (Fig. 2). Molecules with radii $\geq$0.94 nm did not enter the channel ($F \approx 0$) from the *cis* opening and molecules with radii $\geq$0.8 nm did not enter the channel from the *trans* opening, i.e. complete polymer exclusion from the pore was observed. A decrease in polymer size led to an increase in polymer partitioning in a stepwise fashion until an intermediate value ($F^{cis} \approx 0.3$; $F^{trans} \approx 0.1$) was reached. These intermediate values were kept constant for polymers sized from 0.6 nm to 0.8 nm (F^{cis}) and from 0.6 to 0.7 nm (F^{trans}). When the polymer size was further decreased (hydrodynamic radius < 0.6 nm), filling stepwise increased to maximal values (Fig. 2). Thus, complete filling of the channel occurred in two steps, which was interpreted to indicate the presence of vestibules (with cylindrical or cup-shaped geometry at both channel sides) separated by a lengthy constriction. It reflects that the hydrodynamic radii of these polymers are larger than the radius of the constriction, which inhibits polymers from further filling the pore. Such behavior is evidence of a spacious vestibule. The radius of these vestibules (that are assumed to be at each side of the VCC channel) could be equal to the size of the largest PEG on the plateau or larger. The present methodology is unable to resolve this feature in detail.

The independence of the filling on the hydrodynamic radius of polymers has to be observed until the size of the polymers gets smaller than the aperture of the constriction. Since complete filling of the channel occurred when polymers of $r < 0.6$ nm were employed, we conclude that the maximal radius of the constriction approximates this value. The actual radius of the constriction may be smaller (somewhere between 0.3 and 0.6 nm).

The larger entry vestibules have radii which are larger than the largest PEG on the plateau ($r \approx 0.8$ nm for the *cis* vestibule, and $r \approx 0.7$ nm for the *trans* vestibule). Their maximal value can be determined from the *F*-*r* dependences presented in Fig. 2 as the *r*-axis projection of the interception point between the line connecting the filling value for the largest PEG on the intermediate plateau with that for the smallest PEG on the lowest ($F = 0$) invariant value of the dependence. Therefore, we assume that the radius of the *trans* opening of the channel should be close to 0.8 nm. The radius of the *cis* opening appears larger and close to 0.94 nm.

To determine the length of the channel vestibules, the location of the central constriction relative to the openings was analyzed in terms of electrical distance. As developed elsewhere [24], the electrical distance from an opening to the constriction is the ratio of filling seen at the intermediate plateau to the maximal observed filling (F_{max}), i.e. the size of the *cis* vestibule (in electrical distance units, as seen from the *cis* opening) is $= F_{(PEG300\ PEG600)}/F_{max}$, and for the *trans* vestibule(as seen from the *trans* opening) is $F_{(PEG300\ PEG400)}/F_{max}$. If F_{max} is close to 1.0, as in our case, the absolute value of F numerically is close to the value of the electrical distance. For VCC1, the electrical distance was ≈ 0.3 and ≈ 0.1 from the *cis* and *trans* opening, respectively. This means that the *cis* and the *trans* vestibules of the channel (from the

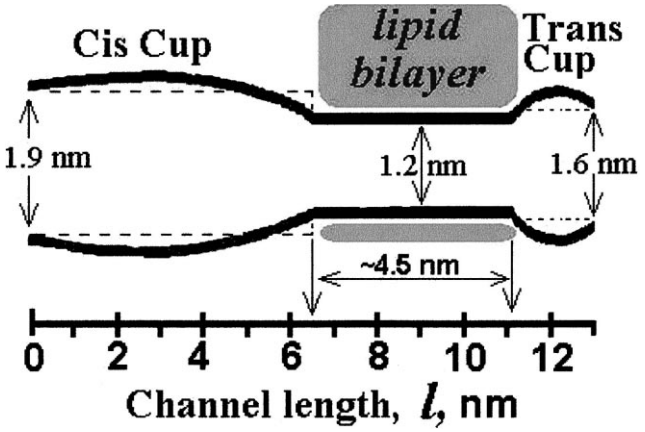

Fig. 3. An inside view on the VCC1 channel lumen and possible channel localization in membrane. *l* is the channel length starting from the *cis* entrance (0 nm) and ending at the *trans* entrance (13 nm). The stretched constriction (diameter ≤1.2 nm) is appeared from ≈6.5 nm to ≈11 nm of the channel length. Channel localization in membrane was deduced based on the similarity between ion channels formed by VCC1 and VCC2 ([18,21], and this study), functional localization of the VCC2 channel *cis* opening in the distance and the *trans* opening in the proximity of the lipid bilayer surface [18] and electron microscopy study demonstrated that the pentameric structure formed with VCC1 is seen as a slightly funnel-shaped structure considerably protruding from the bilayer from the side of the VCC1 addition [43].

opening to the constriction) define ≈30% and ≈10% of the total channel resistance, respectively. The physical length of these different parts of the channel can be calculated: (i) assuming that the inner geometry of all three parts of the channel is roughly cylindrical with radii (r_1, r_2 and r_3) equal to the maximal established (Fig. 2) radii of the *cis* opening, the central constricted part and the *trans* opening, respectively and (ii) accepting that the conductivity of the solutions inside the channel is close to conductivity of the proper bathing solutions. In this case, the transmembrane potential drops through the channel discontinuously although linear at each of its three parts. The total channel resistance (R_{total}) is the sum of three components:

$$R_{cis} + R_{constriction} + R_{trans} =$$

$$(\chi/\pi)[(l_1/r_1^2) + (l_2/r_2^2) + (l_3/r_3^2)]$$

where r_1, r_2 and r_3 are the maximal radius of the *cis* opening, the central constricted part and the *trans* opening established at filling experiments (Fig. 2), and l_1, l_2 and l_3 are the physical length of the *cis* vestibule, the central constriction and the *trans* vestibule, respectively; $l_1+l_2+l_3$ is the total length of the channel and equal to 13 nm as determined by electron microscopy [20]; χ is the conductivity of the solution. Under these assumptions, three other equations can be written: $R_{cis}/R_{total} \approx 0.3$, $R_{trans}/R_{total} \approx 0.1$, $R_{cis}/R_{trans} \approx 3$, which finally permit the calculation of the length of all three parts of the channel. The length of the *cis* vestibule (l_1), the central constriction (l_2) and the *trans* vestibule (l_3) of the channel was estimated to be ≈6.5 nm, ≈4.5 nm and ≈2.0 nm, respectively. From these data the model depicted in Fig. 3 emerges. The *cis* and the *trans* vestibules of the VCC1 channel are depicted here with both cylindrical and cup-shaped geometry because the methodology is not able to distinguish between these two possibilities. The suggested model may be an oversimplification, but it is in basic agreement with electron microscopy data [20], which indicated a funnel-shaped structure of the channel. A cartoon showing the VCC1 channel in the presence of a polymer just at one side is presented in Fig. 4.

4. Discussion

The measurement of nonelectrolyte partitioning into VCC1 channels in bilayer membranes suggests that the pores have an asymmetric geometry. The largest opening of the channel is the *cis* opening with a radius of 0.95 nm. This is in the range (0.7–1.0 nm) deduced from values of VCC1 channel conductance [23] and is similar to the maximal radius of the oligomeric channel created by non-O1 *V. cholerae* cytolysin [18]. The channels formed by both cytolysins have many other features in common. They have moderate selectivity for anions and their I-V curves are sharply asymmetrical. The channels also behave similarly. They both are voltage-gated channels [18,23]. Moreover the potential-induced transition from high to low conductance states increases with decreasing pH. This means that the channels spend much more time in the high conductance state at neutral and weakly alkaline pH, while at acid pH, a fast transition between the states was observed (data not shown). These similarities are consistent with the fact that VCC1 is immunologi-

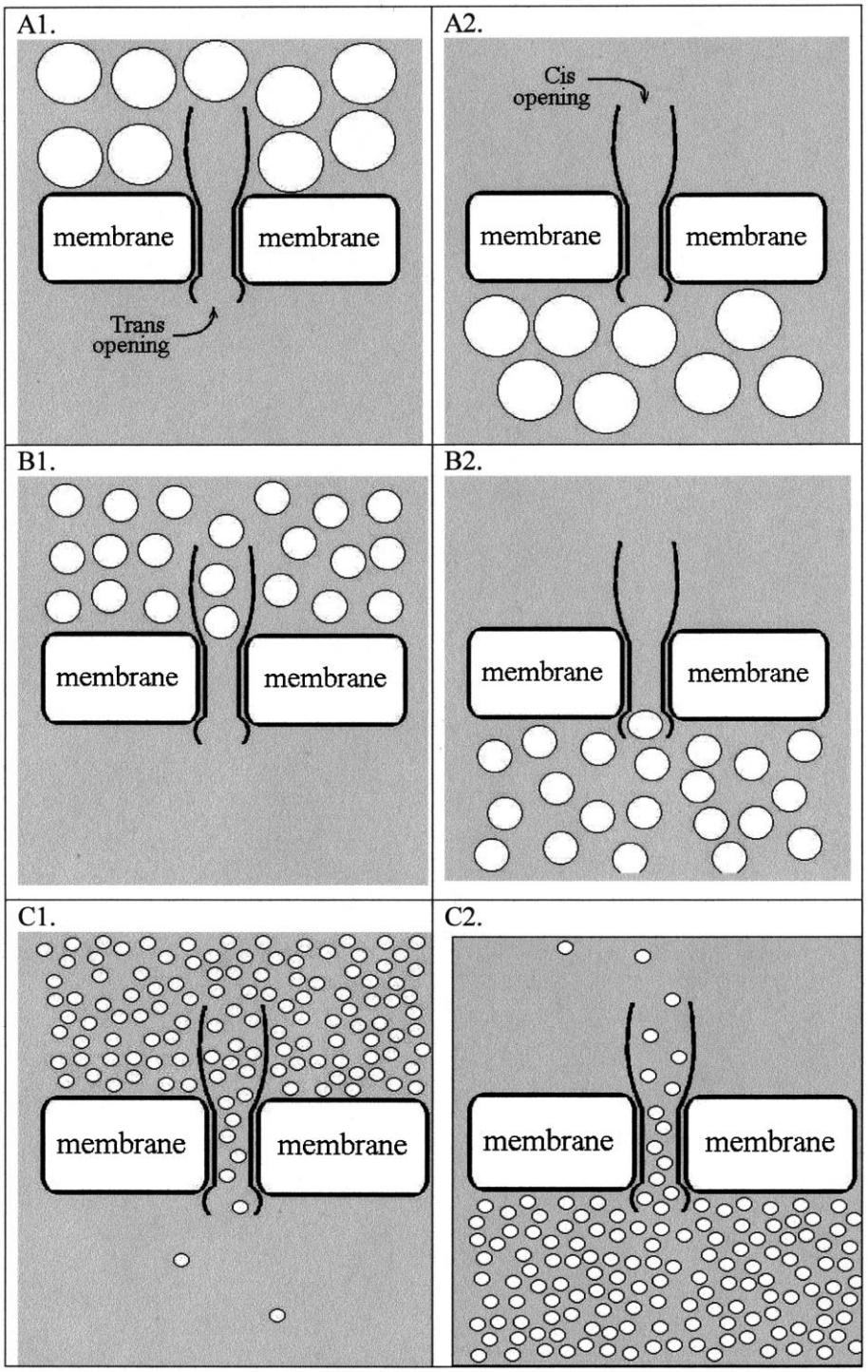

Fig. 4. A cartoon showing the VCC1 channel in the presence of a large (A), medium (B) and small (C) polymer just at one, *cis* (1) or *trans* (2), side. White circles present polymer coils. Large polymer coils do not fill the channel and thus do not change its conductance significantly. Filling is equal to zero. Medium polymer coils are able to fill the appropriate vestibules only. Filling is close to 0.3 and 0.1 in the presence of a polymer from the *cis* and the *trans* opening, respectively. Small polymer coils fill appropriate vestibules and the narrow part of the channel almost completely, meaning that the time-averaged effective polymer concentration inside these two parts of the channel is close to that in a bulk solution. In this case, the opposite (to the side of a polymer addition) channel vestibule is filled particularly. Filling is close to 0.9.

cally related to VCC2 [19] and has nearly identical pH optima for hemolytic activity of the cytolysins [18,21]. The similarities of the properties of VCC1 and VCC2 channels in lipid bilayers and in cell lysis tests suggest that the VCC2 channels could have similar geometry to the channel formed by *V. cholerae* EL Tor cytolysin.

The asymmetry in the I-V curve of VCC1 channels in the fully open state can be particularly explained by asymmetry in lumen geometry. Knowledge of the geometry of VCC1 channels also helps explain the results obtained in hemolytic assays employing the osmotic protection method. It was found [21] that PEG400 ($r = 0.7$ nm) was unable to completely prevent erythrocyte lysis, while PEG600 ($r = 0.8$ nm) did. From these experiments the value for the maximal functional radius of the *V. cholerae* cytolysin channel was determined to be 0.75 nm. This value is almost identical to that established for the size of the smaller *trans* opening of the VCC1 channel in PLMs (see Fig. 2) and not to the size of the constriction zone of the channel ($r \approx 0.6$ nm) established in this study. Perhaps, a reasonable explanation for this discrepancy is the difference in time scale used in bilayer single channel experiments (seconds) and the erythrocyte osmotic balance method (dozens of minutes or hours). As shown recently in experiments with α-toxin channels [27], highly flexible PEG molecules (with Kuhn's length of only several angstroms) behave phenomenologically as hard spheres, enabling their use in channel sizing experiments. Given more time, plasticity of the channel lumen, and more importantly, plasticity of the polymer molecules, make these constrictions 'invisible' and allows all nonelectrolytes that enter the channel to pass through. As recently reported [45], the short-lived, high-amplitude channel blockage could be seen when a single PEG molecule is tethered within the lumen of the α-toxin channel. The blockage could be a result of partial uncoiling of the polymer with consequent chain transition through the constricted part of the channel. In this case, the rate of polymer transport should strongly depend on polymer size, and experiments with tethered PEG3000 and PEG5000 [45] are indeed consistent with the assumption. The rate of polymer transport should also determine the rate of toxin-induced cell lysis: with longer observation times, larger nonelectrolytes will be required to prevent cell lysis. This was experimentally demonstrated for *S. aureus* α-toxin-induced erythrocyte lysis, where only nonelectrolytes that could not enter the channel opening at all protected cells from lysis (O.V. Krasilnikov, unpublished data).

Acknowledgements

We thank Dr. S.D. Aird of the Mestrado em Ciências Fisiológicas at Universidade Estadual do Ceará, for corrections, which improved the clarity of the manuscript. This research was supported by CNPq (Brazil) and by the Deutsche Forschungsgemeinschaft (SFB 490).

References

[1] K. Yamamoto, M. Al-Omani, T. Honda, J. Takeda, T. Miwatani, Non-O1 *Vibrio cholerae* hemolysin purification, partial characterization and immunological relatedness to EL Tor hemolysin, Infect. Immun. 45 (1984) 192–196.

[2] K. Yamamoto, J. Ichinose, N. Nakasone, M. Tanabe, M. Nagahama, J. Sakurai, M. Iwanaga, Identity of hemolysins produced by *Vibrio cholerae* non-O1 and *V. cholerae* 01 biotype EL Tor, Infect. Immun. 51 (1986) 927–931.

[3] R.A. Alm, U.H. Stroeher, P.A. Manning, Extracellular proteins of *Vibrio cholerae* nucleotide sequence of structural gene (hlyA) for the hemolysin of the hemolytic EL Tor strain 017 and characterization of the hlyA mutation in the nonhemolytic classical strain 569B, Mol. Microbiol. 2 (1988) 481–488.

[4] A.E. Rader, J.R. Murphy, Nucleotide sequences and comparison of the hemolysin determinants of *Vibrio cholerae* EL Tor RV79 (Hly^+) and RV79 (Hly^-) and classical 569 B (Hly^-), Infect. Immun. 56 (1988) 1414–1419.

[5] K. Yamamoto, J. Ichinose, H. Shinagawa, K. Makino, A. Nakata, M. Iwanaga, T. Honda, T. Miwatani, Two-step processing for activation of the cytolysin of *Vibrio cholerae* 01 biotype EL Tor nucleotide sequence of the structural gene (HylA) and characterization of processed products, Infect. Immun. 58 (1990) 4106–4116.

[6] K. Nagamune, K. Yamamoto, A. Naka, J. Matsuyama, T. Miwatani, T. Honda, In vitro proteolytic processing and activation of the recombinant precursor of El Tor cytolysin/hemolysin (pro-HlyA) of *Vibrio cholerae* by soluble hemagglutinin/protease of *V. cholerae*, trypsin, and other proteases, Infect. Immun. 64 (1996) 4655–4658.

[7] S. Bhattacharya, A.K. Bose, A.K. Ghosh, Permeability and enterotoxic factors of nonagglutinable vibrios *Vibrio alcaligenes* and *Vibrio parahaemolyticus*, Appl. Microbiol. 22 (1971) 1159–1161.

[8] P.A. Blake, R.E. Weaver, D.G. Hollis, Diseases of humans (other than cholera) caused by vibrios, Annu. Rev. Microbiol. 34 (1980) 341–367.
[9] J.M. Madden, W.P. Nematollahi, W.E. Hill, B.A. McCardell, R.M. Twedt, Virulence of three clinical isolates of *Vibrio cholerae* non-O1 serogroup in experimental enteric infections in rabbits, Infect. Immun. 33 (1981) 616–619.
[10] M. Nishibuchi, R.J. Seidler, D.M. Rollins, S.W. Joseph, Vibrio factors cause rapid fluid accumulation in suckling mice, Infect. Immun. 40 (1983) 1083–1091.
[11] S.G. Williams, S.R. Attridge, P.A. Manning, The transcriptional activator HlyU of *Vibrio cholerae* nucleotide sequence and role in virulence gene expression, Mol. Microbiol. 9 (1993) 751–760.
[12] S.M. Gelbart, M.M. Prabhudesari, *Vibrio cholerae* non-O1 cellulitis, Arch. Pathol. Lab. Med. 110 (1986) 1182–1183.
[13] S. Safrin, J.G. Morris, M. Adams, V. Pons, R. Jacobs, J.E. Conte, Non-O1 *Vibrio cholerae* bacteremia a case report and review, Rev. Infect. Dis. 10 (1988) 1012–1017.
[14] M.H. Lee, H.S. Leu, S.H. Huang, Bacteremic cellulitis caused by non-O1 *Vibrio cholerae* report of case, J. Formos. Med. Assoc. 92 (1993) 472–474.
[15] L.S. Naidu, P.R. Bakerman, M.A. Saubolle, K. Lewis, *Vibrio cholerae* non-O1 meningitis in an infant, Pediatr. Infect. Dis. J. 12 (1993) 879–881.
[16] C. Newman, M. Shepherd, M.D. Woodard, A.K. Chopra, S.K. Tyring, Fatal septicemia and bullae caused by non-O1 *Vibrio cholerae*, J. Am. Acad. Dermatol. 29 (1993) 909–912.
[17] C.H. Shelton, R.L. Martino, K.M. Ramsey, Recurrent non-O1 *Vibrio cholerae* bacteremia in a patient with multiple myeloma, Cancer 72 (1993) 105–107.
[18] O.V. Krasilnikov, J.N. Muratkhodjaev, A.O. Zitzer, The mode of action of *Vibrio cholerae* cytolysin. The influences of both erythrocytes and planar lipid bilayers, Biochim. Biophys. Acta 1111 (1993) 7–16.
[19] A.O. Zitzer, N.O. Nakisbekov, A.V. Li, V.L. Semiotrochev, Yu.L. Kiseliov, J.N. Muratkhodjaev, O.V. Krasilnikov, Yu.V. Ezepchuk, Entero-cytolysin (EC) from *Vibrio cholerae* non-O1 (some properties and pore-forming activity), Int. J. Med. Microbiol. Virol. Parasitol. Infect. Dis. 279 (1993) 494–504.
[20] A. Zitzer, M. Palmer, U. Weller, T. Wassenaar, C. Biermann, J. Tranum-Jensen, S. Bhakdi, Mode of primary binding to target membranes and pore formation induced by *Vibrio cholerae* cytolysin (hemolysin), Eur. J. Biochem. 247 (1997) 209–216.
[21] A. Zitzer, I. Walev, M. Palmer, S. Bhakdi, Characterization of *Vibrio cholerae* EL Tor cytolysin as an oligomerizing pore-forming toxin, Med. Microbiol. Immunol. 184 (1995) 37–44.
[22] Y. Ichinose, K. Yamamoto, N. Nakasone, M.J. Tanabe, T. Takeda, T. Miwatani, M. Iwanaga, Enterotoxicity of EL Tor-like hemolysin of non-O1 *Vibrio cholerae*, Infect. Immun. 55 (1987) 1090–1093.
[23] K. Menzl, E. Maier, T. Chakraborty, R. Benz, HlyA hemolysin of *Vibrio cholerae* O1 biotype EL Tor. Identification of the hemolytic complex and evidence for the formation of anion-selective ion-permeable channels, Eur. J. Biochem. 240 (1996) 646–654.
[24] A. Zitzer, O. Zitzer, S. Bhakdi, M. Palmer, Oligomerization of *Vibrio cholerae* cytolysin yields a pentameric pore and has a dual specificity for cholesterol and sphingolipids in the target membrane, J. Biol. Chem. 274 (1999) 1375–1380.
[25] D.A. Doyle, J.M. Cabral, R.A. Pfuetzner, A. Kuo, J.M. Gulbis, S.L. Cohen, B.T. Chait, R. MacKinnon, The structure of the potassium channel: molecular basis of K^+ conduction and selectivity, Science 280 (1998) 69–77.
[26] O.V. Krasilnikov, J.B. Da Cruz, L.N. Yuldasheva, R.A. Nogueira, A novel approach to study the geometry of the water lumen ion channel. Colicin Ia channels in lipid bilayers, J. Membr. Biol. 161 (1998) 83–92.
[27] P.G. Merzlyak, L.N. Yuldasheva, C.G. Rodrigues, C.M.M. Carneiro, O.V. Krasilnikov, S.M. Bezrukov, Polymeric nonelectrolytes to probe pore geometry: application to the alpha-toxin transmembrane channel, Biophys. J. 77 (1999) 3023–3033.
[28] R. Scherrer, P. Gerhardt, Molecular sieving by the *Bacillus megaterium* cell wall and protoplast, J. Bacteriol. 107 (3) (1971) 718–735.
[29] S. Kuga, Pore size distribution analysis of cell substances by size exclusion chromatography, J. Chromatogr. 206 (1981) 449–461.
[30] O.V. Krasilnikov, R.Z. Sabirov, V.I. Ternovsky, P.G. Merzliak, D.N. Muratchodjaev, A simple method for the determination of the pore radius of ion channels in planar lipid bilayer membranes, FEMS Microbiol. Immunol. 105 (1992) 93–100.
[31] R.Z. Sabirov, O.V. Krasilnikov, V.I. Ternovsky, P.G. Merzliak, Relation between ionic channel conductance and conductivity of media containing different nonelectrolytes. A novel method of pore size determination, Gen. Physiol. Biophys. 12 (1993) 95–111.
[32] M. Montal, P. Mueller, Formation of bimolecular membranes from lipid monolayers and a study of their electrical properties, Proc. Natl. Acad. Sci. USA 69 (1972) 3561–3566.
[33] O.V. Krasilnikov, M.-F.P. Capistrano, L.N. Yuldasheva, R.A. Nogueira, Influence of Cys-130 *S. aureus* alpha-toxin on planar lipid bilayer and erythrocyte membranes, J. Membr. Biol. 156 (1997) 157–172.
[34] R.Z. Sabirov, O.V. Krasilnikov, V.I. Ternovsky, P.G. Merzliak, J.N. Muratkhodjaev, Influence of some nonelectrolytes on conductivity of bulk solution and conductance of ion channels. Determination of pore radius from electric measurements, Biologicheskie Membrany 8 (1991) 280–291.
[35] S.M. Bezrukov, I. Vodyanoy, Probing alamethicin channels with water-soluble polymers. Effect on conductance of channel states, Biophys. J. 64 (1993) 16–25.
[36] S.M. Bezrukov, I. Vodyanoy, V.A. Parsegian, Counting polymers moving through a single ion channel, Nature 370 (1994) 279–281.
[37] S.L. Hager, T.B. MacRury, Investigation of phase-behavior

and water binding in poly(alkylene oxide) solutions, J. Appl. Polymer Sci. 25 (1980) 1559–1571.

[38] C.P.S. Tilcock, D. Fisher, The interaction of phospholipid membranes with poly(ethylene glycol). Vesicle aggregation and lipid exchange, Biochim. Biophys. Acta 688 (1982) 645–652.

[39] J. Breen, D. Huis, J. Bleijser, J.C. Leyte, Solvent dynamic in aqueous PEO-salt solutions studied by nuclear magnetic relaxation, J. Chem. Soc. Faraday Trans. 84 (1) (1988) 293–307.

[40] K.P. Antonsen, A.S. Hoffman, Water structure of PEG solutions by differential scanning calorimetry measurements, in: J.M. Harris (Ed.), Poly(Ethylene Glycol) Chemistry: Biotechnical and Biomedical Applications, Plenum Press, New York, 1992, pp. 15–28.

[41] S.M. Bezrukov, I. Vodyanoy, R.A. Brutyan, J.J. Kasianowicz, Dynamics and free energy of polymers partitioning into a nanoscale pore, Macromolecules 29 (1996) 8517–8522.

[42] S.M. Bezrukov, J.J. Kasianowicz, The charge state of an ion channel controls neutral polymer entry into its pore, Eur. Biophys. J. 26 (1997) 471–476.

[43] J.E. Hall, Access resistance of a small circular pore, J. Gen. Physiol. 66 (1975) 531–532.

[44] O.V. Krasilnikov, R.Z. Sabirov, Ion transport through channels formed by *Staphylococcus aureus* alpha-toxin, Gen. Physiol. Biophys. 8 (1989) 213–222.

[45] S. Howorka, L. Movileanu, X. Lu, M. Magnon, S. Cheley, O. Braha, H. Bayley, A protein pore with a single polymer chain tethered within the lumen, J. Am. Chem. Soc. 122 (2000) 2411–2416.